Frontiers in Heat and Mass Transfer (FHMT), 11, 34 (2018)
DOI: 10.5098/hmt.11.34

Global Digital Central
ISSN: 2151-8629

Frontiers in Heat and Mass Transfer

Available at www.ThermalFluidsCentral.org

SUPERSONIC CONDENSATION CHARACTERISTICS OF CO_2 IN NATURAL GAS UNDER DIFFERENT TEMPERATURE CONDITIONS

Huan Zheng[a,*], Yuliang Ma[b], Huaping Mei[c], Xiaohong Xu[a], Xiguang Chen[d], Xunchen Cao[e]

[a]*School of Geosciences, Yangtze University, Wuhan 430100, China*
[b]*Research Institute of Exploration and Development PetroChina Liaohe Oilfield Company, Panjin 124000, China*
[c]*The Fifth Gas Production Plant, Changqing Oilfield Company, PetroChina, Xi'an 710018, China*
[d]*PetroChina Hangzhou Institute of Petroleum Geology, Hangzhou 310023, China*
[e]*Petroleum Exploration and Development Institute, PetroChina Xinjiang Oilfield Company, Karamay 834000, China*

ABSTRACT

The supersonic separator has proved to be an effective method to condense and separate CO_2 from natural gas, and the inlet temperature plays a vital role on condensation characteristics of CO_2 in the supersonic separator due to the instability temperature of wellhead natural gas. In this paper, the physical and mathematical models for the supersonic condensation process of CO_2 in the natural gas were established on the basis of CO_2 droplet surface tension, nucleation and growth model. The flow and condensation parameters were investigated under different temperature conditions. The results show that when the inlet gas pressure is 8.0 MPa, the inlet gas temperature is 280 K and the CO_2 content is 0.15, the condensation position is x=240.25 mm, the maximum nucleation rate is 1.14×10^{21} $m^{-3}\cdot s^{-1}$, the maximum droplet radius is 2.146×10^{-7} m, the maximum droplet number is 8.20×10^{14} kg^{-1}, and the maximum humidity is 0.0446. The decrease of inlet temperature makes the droplet reach a greater growth rate and a larger radius of droplet at nucleation. With the decrease of the inlet temperature, the condensation position moves forward, the maximum nucleation rate and the droplet number, the droplet radius and the humidity of CO_2 increase.

Keywords: *CO_2, Natural gas, Laval nozzle, Condensation, Temperature*

1. INTRODUCTION

Most of the natural gas contains excessive CO_2 when extracted from the wellhead. If the CO_2 cannot be removed from natural gas, the quality of the natural gas will be affected and the pipeline will be corroded and destroyed. Therefore, CO_2 gas must be removed to meet storage and transportation requirements. Conventional CO_2 removal technologies such as absorption, adsorption, cryogenic separation, and membrane play a positive role and have been widely used in the field of petroleum industry. However, the conventional natural gas processing has proven both costly and complex, requiring large facilities with high operating expenses, and even could cause environment problem (James and Armin, 2007; Chen et al., 2015).

The supersonic separator combines expansion cooling and centrifugal separation in a single compact device with no chemicals requirement, which has widely used for natural gas dehydration and heavy hydrocarbon removal. It is mainly composed of three sections: the Laval nozzle, the long tube integrated with a cyclone, and the diffuser (Liu et al., 2017), as shown in Fig. 1. In the Laval nozzle, the mixture gas adiabatically expands, velocity increases and temperature drops, to promote the condensable gas with formation of droplets. After that, centrifugal effects generated by the cyclone drive the droplets towards the wall of the long tube. Condensed liquid droplets are separated from main gas flow. The remaining dry gas stream flows into the diffuser in which most of the initial pressure is recovered. Compared to the traditional processing, this new device has no moving parts, which ensuring its high reliability and availability. In addition, the supersonic velocity results in an extremely short residence time of the gas-liquids mixture prevents hydrate problems and eliminates the need for chemicals and associated regeneration systems. Therefore, the supersonic swirling separation technology is suited for unmanned operations, e.g., for the oil and gas field in the offshore, desert and remote areas.

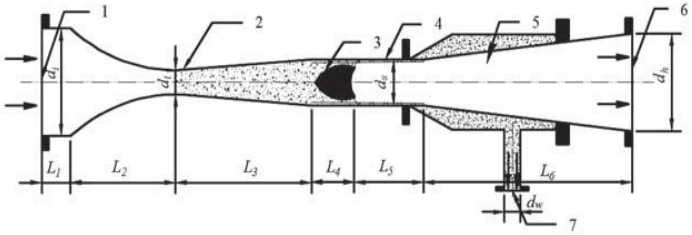

1-Saturated feed gas inlet;2-Laval Nozzle;3-swirling flow generator; 4-straight tube; 5-diffuser section; 6-dry gas outlet; 7-wet gas and slip-gas outlet

Fig. 1 Schematic diagram of the supersonic separator.

In the last few years, some scientific research has focused on structural improvement and condensation process in the supersonic separator. Jassim et al. (2008a and 2008b) and Karimi and Abdi (2009) employed a Laval nozzle to study the single phase flow behavior of natural gas under high pressures. The effects of the nozzle geometry and operating parameters on the flow structure were analyzed using the computational fluid dynamics (CFD) approach. Malyshkina (2008a and 2008b) used the two-dimensional Euler model to study the efficiency of the purification of natural gases. Wen et al. (2011 and 2012) optimized the swirling device and diffuser to investigate flow characteristic, and simulated particle flow numerically in supersonic separator. Xiao et al.

* *Corresponding author. Email: 865651148@qq.com*

DOI: 10.5098/hmt.11.34 ISSN: 2151-8629

(2017) carried out a numerical study the condensing flow characteristics of water vapor in wet natural gas within the Laval nozzle. Bian et al. (2016, 2018a and 2018b) and Jiang et al. (Jiang et al., 2016a) carried out comprehensive research on a newly designed separator, they improved the separator by reducing the expand angle and extending the length of expanding section. Additionally, studies of the supersonic flow and liquefaction process of heavy hydrocarbon component and natural gas in nozzle are also conducted by them.

In recent years, the supersonic separator has been applied to the field of CO_2 removal from natural gas. Bian et al. (2018c) and Jiang et al. (Jiang et al., 2018) investigate the condensation process of CH_4-CO_2 mixture gas and supersonic separation mechanism applying the Discrete Particle Method. In the actual production, due to the instability temperature of wellhead natural gas, the inlet temperature plays a vital role on the separation process of CO_2 in the supersonic separator. However, there is a lack of studies on the effects of inlet temperature on the condensation characteristics of CO_2 and the condensation characteristics are still not clear. Therefore, in this work, the physical and mathematical models for the supersonic condensation process of CO_2 in the natural gas were established on the basis of CO_2 droplet surface tension, nucleation and growth model. On this basis, the effects of inlet temperature on the flow and condensation parameters were investigated.

2. MATHEMATICAL MODEL FOR SUPERSONIC CONDENSATION PROCESS

2.1 Condensation and Surface Tension Model

Assuming that CO_2 is still in the liquid state when the temperature is lower than the triple point (In fact, CO_2 is solid under that circumstance, the separation is much easier to achieve). Girshick and Chiu (1990) and Girshick (1991) proposed classic nucleation theory (CNT) model and internally consistent classical nucleation theory (ICCT) for the droplet condensation process, the studies by Rudek (1996) show that the ICCT is more accurate than the CNT model, so the ICCT model proposed by Girshick is applied to calculate the nucleation rate in this work. The model is described as follows:

$$J = \frac{1}{S}\frac{\rho_v^2}{\rho_l}\sqrt{\frac{2\sigma}{\pi m_o^3}}\exp\left(-\frac{16\pi\sigma^3}{3k_B\rho_l^2 R_M^2 T^2 \ln^2 S}\right)\exp(\theta) \tag{1}$$

Where, J is the droplet nucleation rate; S is the gas supersaturation; ρ_v is the density of the mixed gas; ρ_l is the density of the liquid droplets; σ is the droplet surface tension; m_o is the single molecular mass; k_B is the Boltzmann constant, 1.38×10^{-23}J/K; R_M is the gas constant; T is the temperature of the mixture gas; θ is dimensionless surface tension.

Gyarmathy's model (1996) is employed to calculate the growth rate of droplets, which can be described by Eq. (2).

$$\frac{dr_d}{dt} = \frac{\lambda_v\left(1-\frac{r_c}{r_d}\right)(T_s - T)}{\rho_l h_{lv} r_d\left(1+\frac{2\sqrt{8\pi}}{1.5\,\mathrm{Pr}_v}\frac{\gamma}{\gamma+1}\mathrm{Kn}\right)} \tag{2}$$

where, r_c is the critical radius of the droplet; r_d is the droplet radius; T_s is the saturation temperature of vapor.

The droplet radius is very small (approximately 10^{-9} m) in the droplet growth process and the contact probability with other droplets is very low, so the collision and coalescence between different droplets is ignored in the above models.

The calculation formula of CO_2 surface tension prediction model is calculated by the piecewise function method proposed in the literature (Jiang et al., 2016b). The function combined Pitzer correlation, Zuo-Stenby correlation, Block correlation, Quinn correlation, Miqueua correlation and so on. The average deviation of the piecewise function is only 0.95% compared with the experimental data, which can achieve an accurate prediction of the surface tension of the liquid CO_2.

2.2 Governing Equations

The formation diameter of liquid droplets is very small as mentioned above, so the slip velocity between the vapor and CO_2 droplet is ignored in this paper when the governing equations are established. The vapor flow characteristics in the nozzle are depicted by partial differential equations, including a continuity equation, a momentum equation, and an energy equation, defined as Eqs.(4)-(6). A continuity equation, a droplet number density conservation equation, and a relation about droplet radius, droplet number and humidity are employed to describe the flow characteristics of liquid, presented as Eqs.(7)-(9).

$$\frac{\partial\rho_v}{\partial t} + \frac{\partial}{\partial x_j}\left(\rho_v u_j\right) = S_m \tag{4}$$

$$\frac{\partial}{\partial t}\left(\rho_v u_i\right) + \frac{\partial}{\partial x_j}\left(\rho_v u_j u_i\right) = -\frac{\partial p_v}{\partial x_i} + \frac{\partial}{\partial x_j}\left[\mu\left(\frac{\partial u_j}{\partial x_i} + \frac{\partial u_i}{\partial x_j} - \frac{2}{3}\delta_{ij}\frac{\partial u_j}{\partial x_j}\right)\right] + \frac{\partial}{\partial x_j}\left(-\rho_v\overline{u_i' u_j'}\right) + S_u \tag{5}$$

$$\frac{\partial}{\partial t}\left(\rho_v E\right) + \frac{\partial}{\partial x_j}\left(\rho_v u_j E + u_j p_v\right) = \frac{\partial}{\partial x_j}\left(k_{eff}\frac{\partial T}{\partial x_j} + u_i\tau_{eff}\right) + S_h \tag{6}$$

$$\frac{\partial}{\partial t}\left(\rho_v E\right) + \frac{\partial}{\partial x_j}\left(\rho_v u_j Y\right) = S_Y \tag{7}$$

$$\frac{\partial}{\partial t}\left(\rho_v N\right) + \frac{\partial}{\partial x_j}\left(\rho_v u_j N\right) = J \tag{8}$$

$$r_d = \left(\frac{3Y}{4\pi\rho_l N}\right)^{\frac{1}{3}} \tag{9}$$

where, u_i and u_j are axial and radial velocity components; p is the pressure of the mixed gas; μ is the dynamic viscosity of the mixed gas; δ is the Kronecker delta; u'_i and u'_j are axial and radial velocity fluctuations; E is the total energy; k_{eff} is the effective thermal conductivity; τ_{eff} is the effective stress tensor; ρ is the mixed phase density; m_v is the liquid mass per unit volume condensation in unit time; h is the total enthalpy of gas; h_{lg} is the latent heat of condensation.

The S_m, S_u, and S_h are the source terms of vapor continuity equation, vapor momentum equation and vapor energy equation due to condensation, added to the governing equations.

$$S_m = -m_v \tag{10}$$

$$S_u = -m_v u \tag{11}$$

$$S_h = -m_v\left(h - h_{lg}\right) \tag{12}$$

2.3 Nozzle Structure and Mathematical Model

The supersonic nozzle used in this work is shown in Fig. 2. The whole length of the nozzle is 275.10 mm, the subsonic convergent section and divergent section are 112.02 mm and 63.08 mm, respectively. The diameters of the nozzle inlet, outlet and throat are 70 mm, 18.26 mm and 10 mm, respectively. The curve shape of the convergent section uses bicubic curve and the expanding section adopts circular arc plus linear design method.

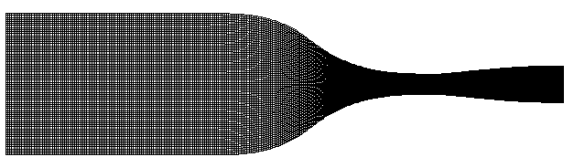

Fig. 2 Grid system for the nozzle.

Global Digital Central
ISSN: 2151-8629

With the continuous development of computer science and technology, computational fluid dynamics has been widely used in many subject areas, including heat and mass transfer, chemical engineering and environmental science. The supersonic condensation characteristics of CO_2 were calculated using the computational fluid dynamics method.

The unstructured meshes are used for the designed structure of the nozzle. A local mesh encryption method is employed at the boundary layer of the nozzle. The inlet and outlet boundary conditions are set respectively according to the flow characteristics of the supersonic compressible gas in the nozzle. The outlet boundary conditions are set to be pressure outlets.

In addition, the wall is with no-slip, no seepage and adiabatic boundary conditions. The grid independence is verified to ensure the accuracy of the results.

In order to ensure accuracy of simulation results, the convergence criterion for the relative residual of the continuity, momentum, energy and all other dependent variables is assigned as 10^{-9}.

2.4 Experimental Verification

The experimental data of Moses and Stein (1978) are used to test the condensation model and numerical method discussed above. The experimental medium is water vapor. The inlet pressure and temperature are 43.023 kPa and 366 K. The comparison of pressure distribution along the nozzle is presented in Fig. 3. As we can see that the predicted and measured onset of the condensation process is in the vicinity of x= 103 mm, and the numerical results are in good agreement with the experimental data especially in the place where the condensation occurs., which illustrates that the models and methods used to simulate the condensation characteristics are suitable.

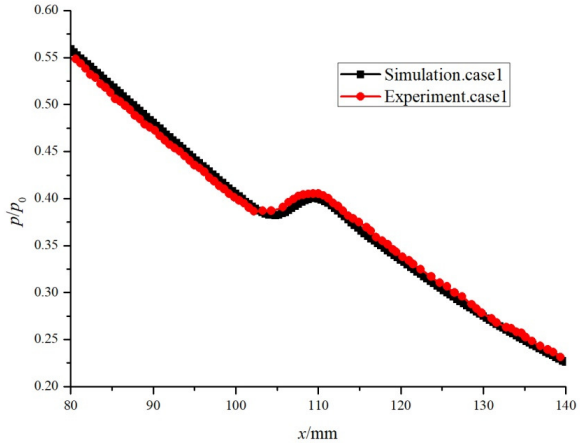

Fig. 3 Comparison between experiment and simulation results in mose's nozzle.

3. EFFECTS OF INLET TEMPERATURE ON CONDENSATION PROCESS OF CO_2 GAS

The influences of inlet temperature on the condensation parameters are numerically simulated, under the conditions that the inlet pressure and water vapor mass fraction are kept constant (8.0 MPa and 0.15, respectively), the inlet temperature is set to be 270 K, 275 K and 280 K, respectively. The flow and condensation parameters distribution (including pressure, temperature, nucleation rate, droplet radius, droplet number humidity, degree of supersaturation and droplet growth rate) in the nozzle were obtained. The results of the simulation are shown in Figs. 4-11.

As we can see from the temperature (Fig.4) and pressure (Fig.5) distribution, when the inlet pressure is 8.0 MPa, volume fraction of the CO_2 is 0.15, with the decrease of the inlet temperature, the condensation position of CO_2 moves forward, but the outlet pressure increases. When the inlet temperature is 280 K, the condensation position is x=240.25 mm and the pressure at outlet is 1.109 MPa, while the condensation position moves to forward to x=226.27 mm and the pressure reaches 1.322 MPa when the inlet temperature is 270 K. This is because with the decrease of inlet temperature, the degree of super-cooling is greater, it is more prone to the realization of condensation. From the pressure distribution we could also see that before the CO_2 gas spontaneous condensation occurs, the pressure distribution is essentially in agreement although the inlet temperature is different, which indicating that the change of inlet temperature has little effect on the temperature when there is no condensation occurs. After that, due to the lower temperature condensation requires a smaller supersaturation, the spontaneous condensation occurs earlier when the inlet temperature is lower.

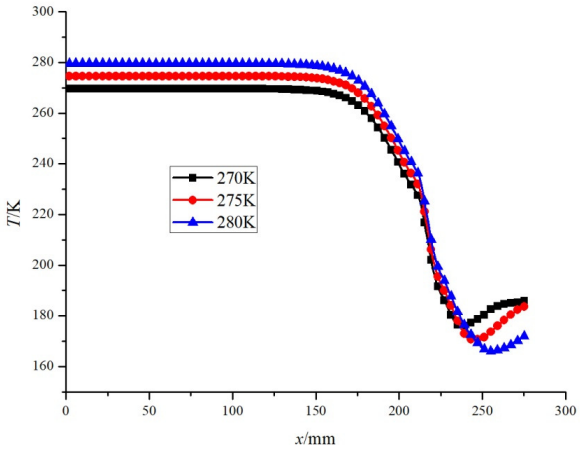

Fig. 4 Temperature distribution in the nozzle.

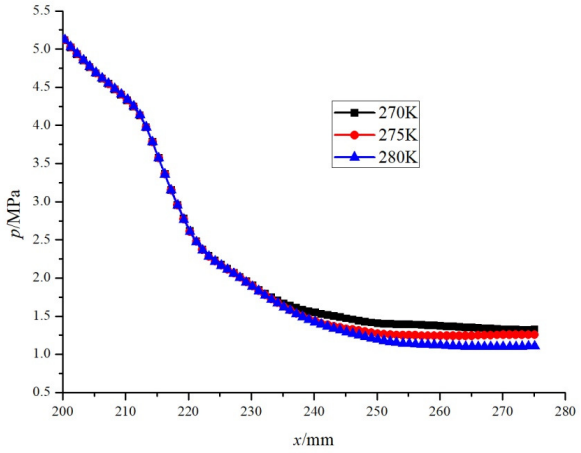

Fig. 5 Pressure distribution in the nozzle.

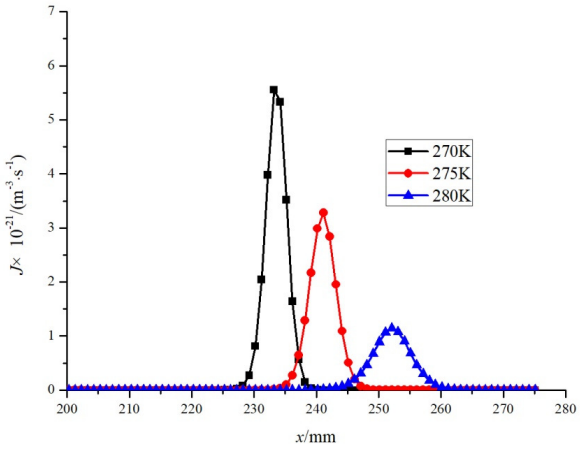

Fig. 6 Nucleation rate distribution in the nozzle.

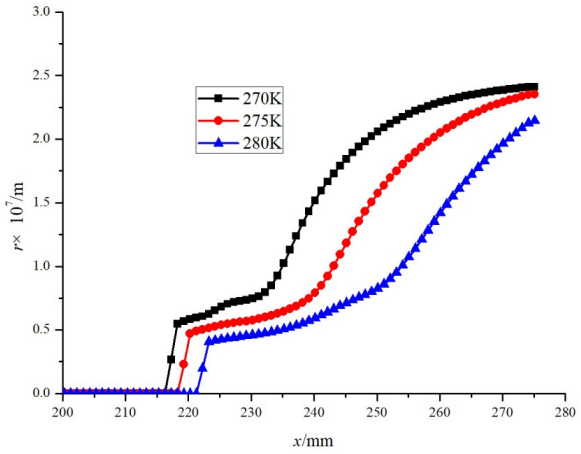

Fig. 7 Droplet radius distribution in the nozzle.

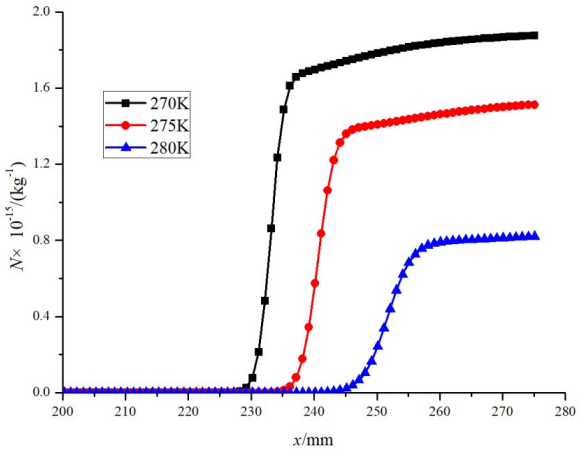

Fig. 8 Droplet number distribution in the nozzle.

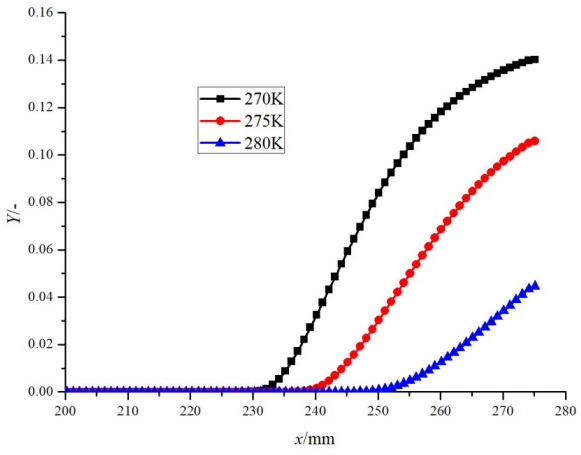

Fig. 9 Humidity distribution in the nozzle.

As we can see from the nucleation rate (Fig.6) and radius (Fig.7) distribution, with the inlet temperature decreases, the maximum nucleation rate and droplet radius increase. When the inlet pressure to 280 K, the maximum nucleation rate is 1.14×10^{21} $m^{-3}\cdot s^{-1}$, and the largest droplet radius is 2.146×10^{-7} m. when the inlet temperature decreases to 270 K, the maximum nucleation rate is 5.55×10^{21} $m^{-3}\cdot s^{-1}$, and the maximum droplet radius increases to 2.411×10^{-7} m. The reason is that the inlet temperature is lower, the position of condensation occurs is in advance, the temperature is higher when condensation occurs, by the formula (1) we can conclude that the nucleation rate is smaller.

From the droplet number (Fig.8) and humidity (Fig.9) distribution under different temperature conditions we can see, with the decrease of inlet temperature, the droplet number and humidity of CO_2 increases gradually. When the inlet temperature is 280 K, the maximum droplet number is 8.20×10^{14} kg^{-1}, the outlet humidity is 0.0446, but when the inlet temperature decreases to 270 K, the maximum droplet number increases to 1.87×10^{15} kg^{-1}, the outlet humidity increases to 0.1403.

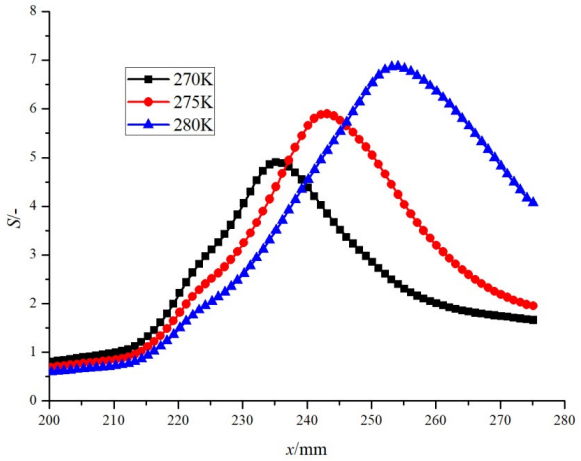

Fig. 10 Degree of supersaturation distribution in the nozzle.

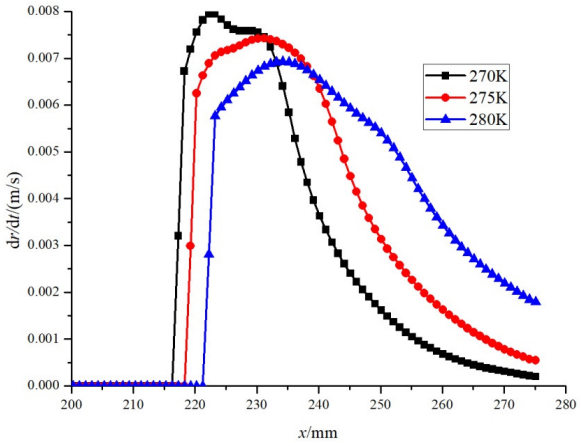

Fig. 11 Droplet growth rate distribution in the nozzle.

It can be seen in combination with all the results, the decrease of inlet temperature makes the droplet reach a greater growth rate and a larger radius of droplet at nucleation. However, as the condensation promotes more condensation heat release, the decrease of the degree of supersaturation and the droplet growth rate are faster, and the droplet radius slows down when the condensation occurs. The reduction of inlet temperature plays a leading role in the promotion of condensation, and greater humidity can be reached at the outlet of the nozzle. When the inlet temperature is 270 K, the outlet humidity of the nozzle is 0.1403, which is equivalent to 70.15% of CO_2 liquefied, and the mole fraction of CO_2 in the outlet gas decreases to 0.0597.

4. CONCLUSIONS

When the inlet gas pressure is 8.0 MPa, the inlet gas temperature is 280 K and the CO_2 content is 0.15, the condensation position is x=240.25 mm, the maximum nucleation rate is 1.14×10^{21} $m^{-3}\cdot s^{-1}$, the maximum droplet radius is 2.146×10^{-7} m, the maximum droplet number is 8.20×10^{14} kg^{-1}, and the maximum humidity is 0.0446.

The decrease of inlet temperature makes the droplet reach a greater growth rate and a larger radius of droplet at nucleation. However, as the condensation promotes more condensation heat release, the decrease of the degree of supersaturation and the droplet growth rate are faster, and

Global Digital Central
ISSN: 2151-8629

the droplet radius slows down when the condensation occurs. The reduction of inlet temperature plays a leading role in the promotion of condensation, and greater humidity can be reached at the outlet of the nozzle.

With the decrease of the inlet temperature, the condensation position moves forward, the maximum nucleation rate and the droplet number, the droplet radius and the humidity of CO_2 increase. In the actual production, the condensation of CO_2 in natural gas can be promoted by adjusting the inlet temperature, and the liquefaction efficiency of the Laval nozzle will be improved.

ACKNOWLEDGEMENTS

This study was supported by the National Natural Science Foundation of China (Grant No. 51406257).

NOMENCLATURE

a_0	molecular surface area [m^2]
E	total energy [J kg^{-1}]
h	vapor total enthalpy [J kg^{-1}]
h_{lg}	latent heat of condensation [J kg^{-1}]
J	spontaneous nucleation rate, [m^{-3} s^{-1}]
K_r	heat transfer coefficient between the droplet and the surrounding vapor [J K^{-1}]
k_B	Boltzmann constant [J K^{-1}]
k_{eff}	effective thermal conductivity [W (m K) $^{-1}$]
Kn	Kundsen number [-]
l_2	length of expanding section [mm]
m_v	liquid mass per unit volume condensation in unit time [kg m^{-3} s^{-1}]
m_o	single molecular mass [kg]
N_A	Avogadro's constant [mol^{-1}]
p	gas pressure [Pa]
p_c	critical pressure [bar]
Pr_v	Prandtl number [-]
r	radius at arbitrary cross section of x [mm]
r_c	critical radius of droplets, [m]
r_{cr}	radius of the nozzle throat [mm]
r_d	Sauter radius of droplets, [m]
R_M	gas constant, [J kg^{-1} K^{-1}]
S	degree of supersaturation[-]
S_m	vapor continuity equation source term [kg m^{-3} s^{-1}]
S_u	vapor momentum equation source term [kg m^{-2} s^{-2}]
S_h	vapor energy equation source term [J m^{-3} s^{-1}]
S_Y	liquid continuity equation source term [kg m^{-3} s^{-1}]
t	temperature in the current state [°C]
T	gas temperature [K]
T_c	critical temperature [K]
T_s	saturation temperature of vapor [K]
u	gas velocity [m s^{-1}]
u'	velocity fluctuation [m s^{-1}]
V_c	critical volume [m^3 mol^{-1}]
v_l	volume of a single droplet [m^3]
x	distance between arbitrary cross section and the inlet [mm]
Y	humidity [-]
Greek symbols	
δ	Kronecker delta [-]
μ	dynamic viscosity of the mixed gas [N s m^{-1}]
ρ	mixed phase density [kg m^{-3}]
ρ_v	mixed gas density [kg m^{-3}]
ρ_l	liquid density [kg m^{-3}]
σ	surface tension of droplets [N m^{-1}]
σ_0	liquid surface tension at 0°C [N m^{-1}]
σ_r	comparative surface tension when the dual reference fluid contrast state method is used [N m^{-1}]
θ	dimensionless surface tension [-]
κ	Boltzmann constant, κ=1.38×10^{-23} [J/K]
τ_{eff}	effective stress tensor [-]
φ	the expansion angle [degree]
λ_v	thermal conductivity of the vapor [$Wm^{-1}K^{-1}$]
γ	specific heat ratio of the vapor phase [-]
ω	eccentricity factor [-]

REFERENCES

Bian, J., Jiang, W. M., Teng, L., Liu Y., Wang S. W., and Deng Z. F., 2016, "Structure improvements and numerical simulation of supersonic separators," Chemical Engineering and Processing: Process Intensification, **110** (5), 214-219.
https://doi.org/10.1016/j.cep.2016.10.012

Bian, J., Cao, X. W., Yang, W., Edem M. A., Yin P. B., and Jiang W. M., 2018a, "Supersonic liquefaction properties of natural gas in the Laval nozzle," Energy **159** (9), 706-715.
https://doi.org/10.1016/j.energy.2018.06.196

Bian, J., Cao, X. W., Yang, W., Du H., and Yin P. B., 2018b, "Effects of external particles on the liquefaction property of natural gas in a Laval nozzle," Powder Technology, **339** (11), 894-902.
https://doi.org/10.1016/j.powtec.2018.08.077

Bian, J., Jiang, W. M., Hou, D. Y., Liu Y., and Yang J, 2018c, "Condensation characteristics of CH_4-CO_2 mixture gas in a supersonic nozzle," Powder Technology, **329** (1), 1-11.
https://doi.org/10.1016/j.powtec.2018.01.042

Chen, X. Y., Vinh-Thang, H., Ramirez, A. A., 2015, "Membrane gas separation technologies for biogas upgrading," Rsc Advances, **5** (31), 24399-24448.
https://doi.org/10.1039/c5ra00666j

Girshick, S. L., and Chiu, C. P., 1990, "Kinetic nucleation theory: a new expression for the rate of homogeneous nucleation from an ideal supersaturated vapor," Journal of Chemical Physics, **93** (9), 1273-1277.
https://doi.org/10.1063/1.459191

Girshick, S. L., 1991, "Comment on: self-consistency correction to homogeneous nucleation theory," Journal of Chemical Physics, **94** (1), 826-827.
https://doi.org/10.1063/1.460309

Gyarmathy, G., 1982, "The spherical droplet in gaseous carrier streams: review and synthesis," Multiphase Science & Technology **1** (2), 99-279.
https://doi.org/10.1615/MultScienTechn.v1.i1-4.20

James, A. R., and Armin, D. E., 2007, "State-of-the-art adsorption and membrane separation processes for hydrogen production in the chemical and petrochemical industries," Separation Science & Technology, **42** (6), 1123-1193.
https://doi.org/10.1080/01496390701242194

Jassim, E., Abdi, M. A., and Muzychka, Y., 2008, "Computational fluid dynamics study for flow of natural gas through high-pressure supersonic nozzles: part 1. Real gas effects and shockwave," Petroleum Science and Technology, **26** (15), 1757-1772.
https://doi.org/10.1080/10916460701287847

Jassim, E., Abdi, M. A., and Muzychka, Y., 2008, "Computational fluid dynamics study for flow of natural gas through high-pressure supersonic nozzles: part 2. Nozzle geometry and vorticity," Petroleum Science and Technology, **26** (15), 1773-1785.
https://doi.org/10.1080/10916460701304410

Global Digital Central
ISSN: 2151-8629

Jiang, W. M., Bian, J., Wu, A., Gao S., Yin P. B., and Hou D. Y., 2018, "Investigation of supersonic separation mechanism of CO_2 in natural gas applying the Discrete Particle Method," Chemical Engineering and Processing: Process Intensification, **123** (2), 272-279.
https://doi.org/10.1016/j.cep.2017.11.019

Jiang, W. M., Bian, J., Liu, Y., Liu Z. L., Teng L., and Geng G., 2016a, "Investigation of flow characteristics and the condensation mechanism of ternary mixture in a supersonic nozzle," Journal of Natural Gas Science and Engineering. **34** (15), 1054- 1061.
https://doi.org/10.1016/j.jngse.2016.07.075

Jiang, W. M., Bian, J., Liu, Y., Gao S., Chen M. C., and Du S. L., 2016b, "Modification of the CO_2 surface tension calculation model under low-temperature and high-pressure condition," Journal of Dispersion Science & Technology, **38** (5), 671-676.
https://doi.org/10.1080/01932691.2016.1188399

Karimi, A., and Abdi, M. A., 2009, "Selective dehydration of high-pressure natural gas using supersonic nozzles," Chemical Engineering and Processing: Process Intensification, **48** (9), 560-568.
https://doi.org/10.1016/j.cep.2008.09.002

Liu, X. W., and Liu, Z. L., 2017, "Numerical investigation and improvement strategy of flow characteristics inside supersonic separator," Separation Science & Technology, **53** (4), 940-952.
https://doi.org/10.1080/01496395.2017.1388256

Malyshkina, M. M., 2008, "The structure of gas dynamic flow in a supersonic separator of natural gas," High Temperature, **46** (7), 69-76.
https://doi.org/10.1134/s10740-008-1010-5

Malyshkina, M. M., 2008, "The procedure for investigation of the efficiency purification of natural gases in a supersonic separator," High Temperature, **48** (15), 244-250.
https://doi.org/10.1134/S0018151X10020161

Moses, C. A., and Stein, G. D., 1978, "On the growth of steam droplets formed in a Laval nozzle using both static pressure and light scattering measurements." Journal of Fluids Engineering, **100** (3), 311.
https://doi.org/ 10.1115/1.3448672

Rudek, M. M., Fisk, J. A., Chakarov, V. M., and Katz J. L., 1996, "Condensation of a super-saturated vapor. Xii. The homogeneous nucleation of the n-alkanes," Journal of Chemical Physics, **105** (4), 4707-4713.
https://doi.org/10.1063/1.472312

Wen, C., Cao, X. W., Yang, Y., and Li W. L., 2012a, "Numerical simulation of natural gas flows in diffusers for supersonic separators," Energy **37** (5), 195-200.
https://doi.org/10.1016/j.energy.2011.11.047

Wen, C., Cao, X. W., Yang, Y., and Zhang J., 2012b, "Evaluation of natural gas dehydration in supersonic swirling separators applying the Discrete Particle Method," Advanced Powder Technology, **23** (4), 228-233.
https://doi.org/10.1016/j.apt.2011.02.012

Xiao, R., Jin, W., Han, S., Rui L., and Cao X. W., 2017, "Numerical simulation on condensing flow of water vapor of wet natural gas inside the nozzle," Frontiers in Heat & Mass Transfer, **9**, 6, 1-8.
http://dx.doi.org/10.5098/hmt.9.6